Chapter 15
Increased Antimicrobial Activity of Cheese Coatings Through Particle Size Reduction

Gabriel M.H. Meesters and Stephen L.A. Hennart

Abstract This chapter discusses the results of reducing the particle size distribution of an anti-microbial solid to facilitate a better use of the material. The product, an antifungal agent is size reduced using a wet-stirred media mill. The obtained product has the size of around 180 nm. The way of grinding is described and the used sizing techniques discussed. In the last part the product is characterized and tested in its application. Here it is shown that the reduced size gives a better performance against fungal anti-microbial infections than a product containing larger particles. This is explained by discussing the coverage, as well as the diffusion of the product through a layer of material, in this case a cheese surface.

15.1 Introduction

This chapter focuses on food coatings such as cheese coatings. A preservative additive is often incorporated in the coating to prevent microbial growth in the food products. The shelf life of the food product is defined as the time without any microbial growth. The preservative being poorly water soluble is mainly present in the form of particles. These slowly dissolve and the dissolved molecules diffuse into the coating.

The approach reviewed in this chapter is to reduce the particle size of the preservative particles in the coating and to prove that the size of the particles and the efficiency of the antimicrobial agent are correlated. At a given concentration, both the number of particles and the total surface area of product available increase with decreasing particle size. This enables one to reduce the distances between the

G.M.H. Meesters (✉) • S.L.A. Hennart
DSM Food Specialities, Alexander Fleminglaan 1, 2613 AX Delft 1, Delft 2600 MA, The Netherlands
e-mail: gabrie.meesters@DSM.com; Stephen.Hennart@qiagen.com

H.G. Merkus and G.M.H. Meesters (eds.), *Particulate Products: Tailoring Properties for Optimal Performance*, Particle Technology Series 19,
DOI 10.1007/978-3-319-00714-4_15,

particles. The increase in specific surface area improves the product dissolution rate. At a given concentration in the food coating, the product diffuses along shorter distances when decreasing product particle size. This will improve the shelf life of the food product by a better antimicrobial action.

The example taken in this chapter is a product named Plasticoat®, produced by DSM Food Specialties, The Netherlands. Plasticoat® is used as cheese coating and contains a poorly soluble antifungal active product. The antifungal compound is active only in dissolved state.

15.1.1 Antimicrobial Protection of Food Surfaces

Gustavsson et al. [18] reported in 2011 that "roughly one-third of food produced for human consumption is lost or wasted globally, which amounts to about 1.3 billion tons per year". One of the causes of food waste is fungal growth that shortens shelf life.

In the food industry several research groups are working on the protection of food and food surfaces against mold growth. The challenges are optimization of the protection systems to enhance the shelf life of food products. In various studies reported by Teerakarn et al. [43], Gill et al. [13], Vojdani et al. [46], Ouattara et al. [36], Warin et al. [47], Ozdemir and Floros [37, 38] the food surface is protected by a coating containing antimicrobial products. The antimicrobial product is often a poorly soluble solid crystalline compound. So a large part of the active molecules is in a particulate form. The antimicrobial particles are dispersed in the coating.

From the previous research cited above it is known that the different aspects regulating the concentration of the product in the coating are product diffusion, product dissolution, particle distribution, product degradation and the sensitivity of the microbe to the product (minimum concentration necessary to inhibit the growth of the organism).

The present work is based on the idea that the particle size has an influence on the shelf life of a food product protected by a film which contains the antimicrobial particles. Indeed, a reduction in particle size should increase the product specific surface area and the number of particles per unit of coating surface area. The particle surface area has an influence upon the dissolution properties and upon the product diffusion. The number of particles has influence on the distribution of particles in the coating. The smaller the particles the more influence of the parameters is to be expected.

15.1.2 Production of Sub-Micrometer Particles

Different methods are available to produce small particles. Particles can be obtained by bottom up approaches like controlled precipitation or cryogenic spraying for example. The inverse approach – top-down – consists in particle size reduction by milling.

Published research shows a large potential of wet ball milling to produce sub-micrometer particles. Inorganic material, like aluminum particles and some organic pigments particles are, for example, reduced to the sub-micrometer size range. Very fine powders of inorganic products, for example silica particles or metals, are produced by grinding in wet ball mills. Grinding enables, in such applications, a particle size reduction to less than 50 nm. Inorganic surfactants are used to prevent agglomeration of nano-particles.

Grinding of organic products is studied in the pharmaceutical industry. In most cases, grinding is carried out using additives such as polymers or cyclodextrines [14, 22]. Those additives enable finer grinding, better physical stability and/or chemical stability. An example is given by Horter and Dressman [23]. When the dissolution process is a rate-determining step, an improvement in the dissolution rate of poorly water-soluble drugs is required for enhancement of the gastrointestinal absorption. Grinding with polymers is known to be one pharmaceutical approach to improve the dissolution rate of drugs [34, 42, 45, 48] and may be useful for enhancement of the gastrointestinal absorption of poorly water-soluble drugs. The polymer acts as a surfactant to enhance the physical stability of the ground particles.

Stirred media mills are therefore expected to be capable of reducing the particle size of antimicrobial products to be used in the food coatings. Many polymers used in the pharmaceutical industry do not have a food grade status. Where grinding without additives is possible, costs are limited and no toxicological issues are raised.

15.1.3 Characterization of the Particle Stability

As shown by Mende et al., after grinding the particles can form agglomerates, which is undesirable [11, 26, 33]. Focus is required on the prevention of agglomeration after wet grinding of poorly soluble crystalline organic compounds.

When two colloidal particles approach one another, attractive and repulsive forces come into play. Particles can approach each other because of Brownian motion and convective transport. The main attraction and repulsion forces are the van der Waals force and the electrostatic interaction force, respectively.

The research by Mende et al. on sub-micron grinding of inorganic products shows that the stability of the product and its final particle size are a function of the electrostatic properties of the particles (zeta-potential) and therefore of the pH of the solution [33].

The detection of agglomerates is, in practice, not always straightforward. Different particle sizing techniques can give different results depending on the measurement conditions. Imaging techniques enable a visual representation of the agglomerates in suspension. Sedimentation measurements are another approach to the characterization of the agglomerates.

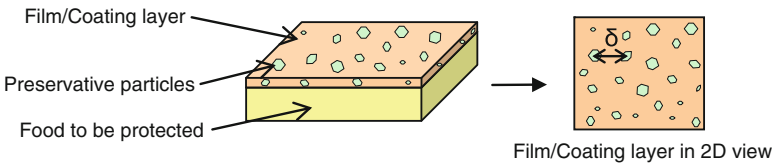

Fig. 15.1 Schematic view of the studied particle dispersion in a coating and its equivalent 2D representation (δ is the variable distance between the particles in the coating distance between particles)

15.1.4 Application of Particles in Coatings on Food Surfaces

As mentioned the different aspects regulating the concentration of the preservative in the coating are diffusion, degradation, dissolution, the particle distribution and the sensitivity of the mold to the preservative. Accelerated shelf life tests are used to experimentally investigate the influence of particle size on shelf life.

The present chapter explains the behavior of a poorly water soluble preservative coated onto food surfaces and describes the effect of product particle size on shelf life of a food product. Figure 15.1 illustrates the studied system.

15.2 Production of Sub-Micrometer Particles

15.2.1 Grinding Process

This part focuses on the grinding of the poorly water soluble antifungal crystalline compound. The material has a starting mean product particle size ($D_{4,3}$) of 15 μm; its density is of 1,300 kg.m^{-3}. Grinding was performed using a ball mill (Dynomill, Bachofen AG, Switzerland). These grinding experiments have been performed in the absence of additives. Particle size distributions have been measured with a laser diffraction size analyzer (LS230 equipment from Beckman Coulter).

The ball mill was operated in a recirculation mode. The poorly water soluble organic product was suspended in water (4.8 % w/w, 500 mL solution). Figure 15.2 shows the circulation of the product suspension through the grinding chamber (volume of the chamber: 300 mL, pump speed: 2 mL.s^{-1}) that was filled at 80 % (bulk volume) with grinding beads (Zirconium oxide, Yttrium stabilized beads from Tosoh, Japan). The product suspension was extracted through a 0.1 mm gap to prevent the grinding medium exiting the milling chamber. The system was cooled to keep a constant temperature throughout the entire system.

The particle size distribution was measured as a function of time throughout the grinding process. Figure 15.3 shows an example of data that were obtained during a grinding experiment.

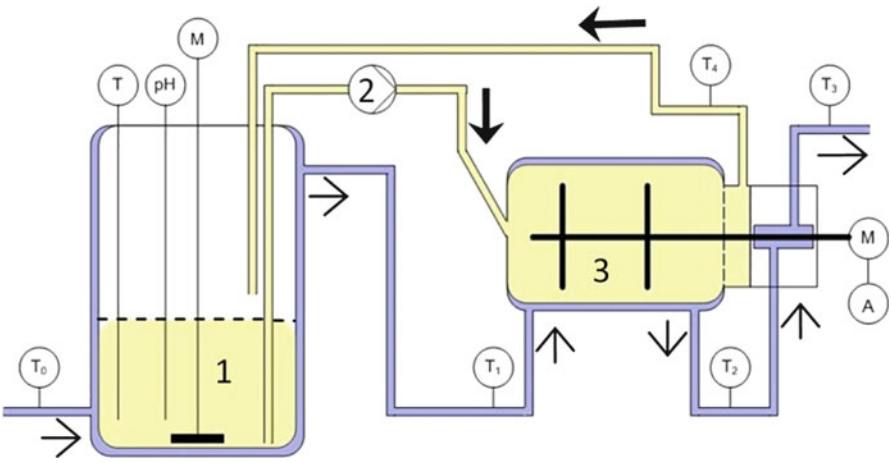

Fig. 15.2 Grinding set-up and controls, where *T* is a temperature measurement and pH is a pH control point. Arrows show the circulation of the cooling water (→) and product (➔). The product is pumped from the stirred tank marked as 1 by the pump 2 to the grinding chamber 3. M stands for motor and A for Amp meter

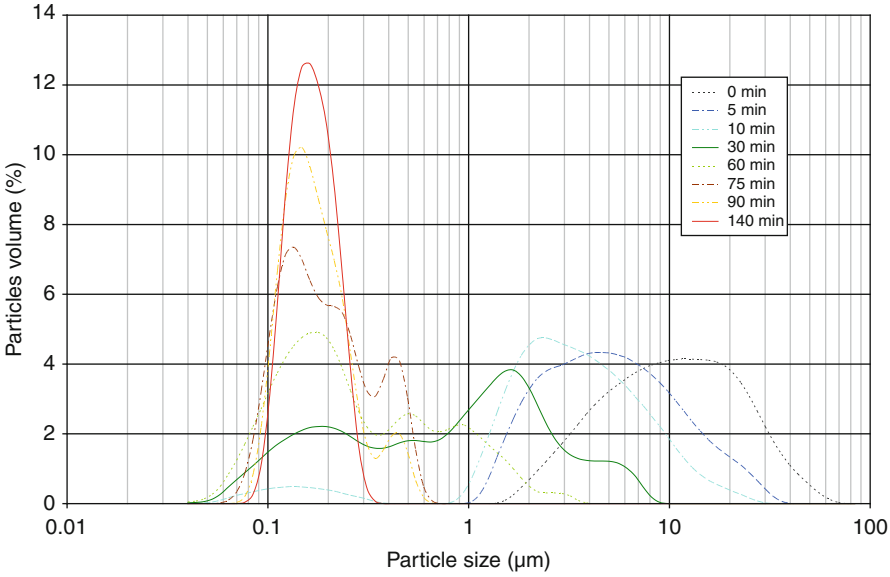

Fig. 15.3 Evolution of the particle size distribution as function of the grinding time (process parameters: rotation speed: 2,000 rpm, grinding media size: 0.5 mm)

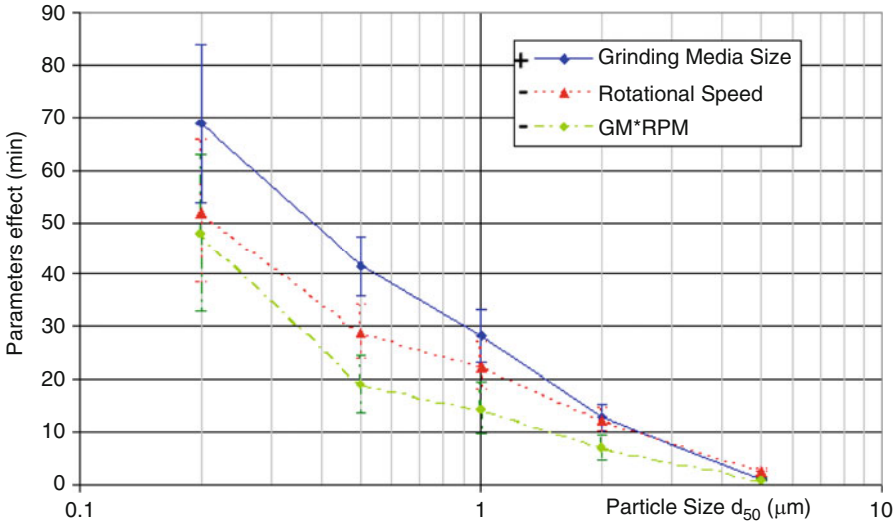

Fig. 15.4 Effect of grinding medium bead size, rotational speed and final product particle size (d_{50}) on grinding time. Effects can be positive (+) or negative (−). As example, the effect of grinding media size is negative (−): the bigger the grinding media size, the longer the grinding time

15.2.2 The Effect of Grinding Medium Bead Size and Rotational Speed on Grinding Time

The first objective was to analyze the effect of grinding medium bead size and rotational speed on grinding time on the basis of factorial design. The calculations were done using Statgraphics 5.1 software ANOVA (ANalysis Of VAriance). The effect was measured as the average response at a high parameter value minus the average response at a low parameter value. Figure 15.4 shows that the influence of grinding medium bead size and rotational speed on grinding time increases exponentially as the final product particle size decreases. The influence of these parameters on grinding time is thus very strong, especially when sub-micrometer product particles are desired.

The influence of rotational speed alone, and the product of rotational speed and grinding medium bead size is negative (negative in this case implies shorter grinding time). Thus, at higher rotational speed, a shorter grinding time is required. Opposite to this the grinding medium bead size has a positive effect on grinding time, i.e. smaller grinding beads give a shorter grinding time to reach a certain product particle size.

The data from Fig. 15.4 can be normalized. The normalized effect of one parameter is the ratio of the effect of that parameter and the sum of the effects from all parameters. Figure 15.5 shows the normalized data in order to compare the

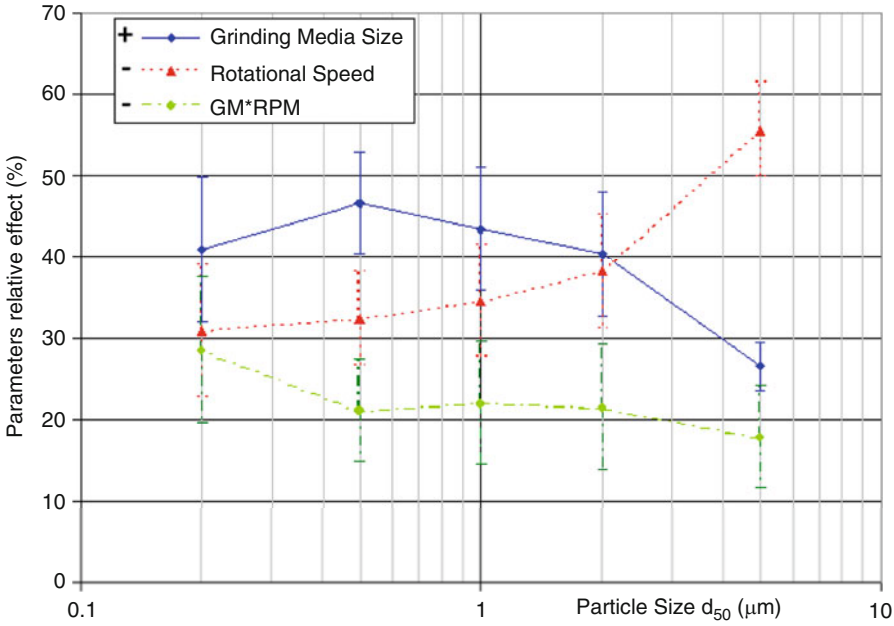

Fig. 15.5 Relative effect of the different parameters and combination of parameters on the time of grinding to reach different particle sizes

relative effects of the grinding parameters. The rotation speed is the dominant factor for grinding in the median particle size range above about 2 um, but its influence decreases in the sub-micrometer range. The bead size of the grinding medium becomes dominant for reaching median particle sizes in the sub-micrometer range.

The strongest effect of the rotation speed is observed in the coarse product size range and the finer product size range is less influenced by the speed. This is confirmed by the observations from Jankovic [27] and Hou et al. [24], the relative effect of the rotation speed is decreasing with the product particle size.

15.2.3 The Effect of Grinding Medium Bead Size and Rotational Speed on Heavy Metal Contamination

The forces applied in the grinding chamber are of great magnitude and high frequency. The stainless steel grinding chamber and the grinding medium (zirconium oxide stabilized with yttrium) undergo wear. Heavy metals can therefore enter the final suspension. Stainless steel is typically composed of iron, chromium, nickel and carbon. Carbon contamination cannot be detected since the ground product is organic and contains carbon atoms. The focus was therefore on the heavy metals. The content of iron, chromium, nickel and zirconium was determined using an atomic absorption

Table 15.1 Heavy metal content after 3 h grinding (ppm, ± 0.05 ppm)

d_{GM} (mm)	v_{tip} (rpm)	Zr	Cr	Fe	Ni
0.8	6,000	103	80	295	59
0.8	2,000	9.9	1.7	6.8	1.5
0.3	6,000	56	20	73	15
0.3	2,000	7.9	0.29	1.8	0.6

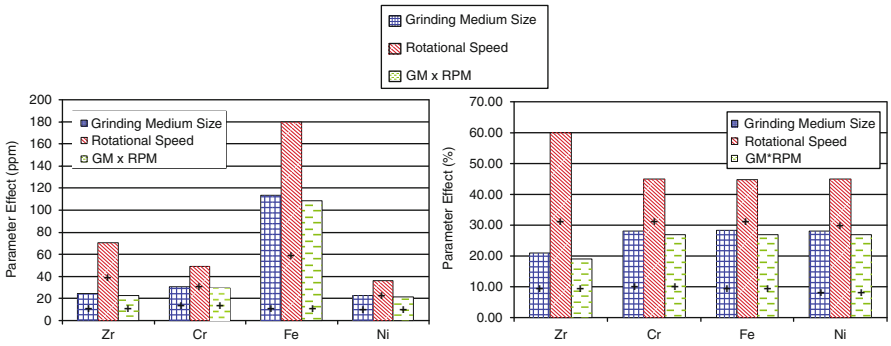

Fig. 15.6 Parameter effect (*left*) and relative effect (*right*) of grinding medium size and rotational speed on the heavy metal contamination after 3 h grinding

spectrophotometer. Table 15.1 shows the influence of the rotational speed, v_{tip}, and the grinding medium bead size, d_{GM}, on the heavy metal content.

The contamination by heavy metals is strongly dependent on the grinding conditions and the material hardness. The contamination by zirconium and iron ranges from a few ppm to a couple of hundreds ppm; the chromium and nickel contents are somewhat smaller. The contamination by zirconium is limited because the grinding medium is relatively hard in comparison to the grinding chamber that is composed of stainless steel. Table 15.1 and Fig. 15.6 present the heavy metal contamination after 3 h of grinding. The required grinding time to reach a specific product particle size may be shorter than 3 h. Contamination levels can therefore be reduced in some cases. An optimum balance needs to be found between heavy metal contamination and the product particle size that is reached. The biggest impact is found for the rotation speed. At higher speeds the heavy metal concentrations increase. The effect of the grinding medium bead size is less important. The number of impacts between the grinding beads and the grinding chamber wall thus seems to have a smaller impact than the collision force.

The results from Breitung-Faes et al. [5] showed that the bigger the grinding media the more contamination would occur. This effect is seen here and it is very limited. The hardness of the product material as mentioned by Becker and Schwedes [1] determines the bead wear as well. The present organic product milled is presumed to be much softer than a metal or ceramics (as used in the references) and thus the wear of the grinding media is very limited.

The conclusions from Howorth [25] are consistent with the present observation. Howorth indicated that the harder the medium, the less contamination would be

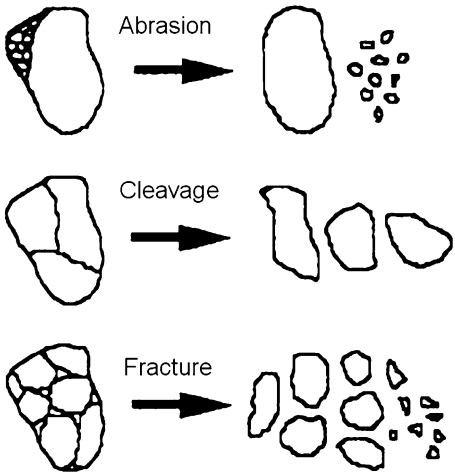

Fig. 15.7 Fragmentation mechanisms (Adopted from Varinot et al. [44])

detected. The present experiments are carried out with zirconium oxide, which is one of the hardest materials used as grinding media. Its wear is according to Howorth and, as observed here, is very limited.

The stainless steel composition is constant. Wear should therefore be similar for all metals that are present in stainless steel. This is confirmed by Fig. 15.6.

15.2.4 Breakage Mechanisms

The nature and the intensity of the applied stresses on the particles affect the particle size reduction process. In comminution the following three main breakage mechanisms have been identified (Fig. 15.7) [2, 4, 19, 41]:

- Abrasion occurs when stress is applied on particles along the tangential axis (shear). Particle breakage in this case gives a bimodal particle size distribution comprising fine particles that are released from the surface of the initial particles, in addition to particles with a size close to that of the initial particles.
- Cleavage of particles occurs when intense stresses are slowly applied on a particle (compression). This produces fragments of sizes 50–80 % v/v smaller than the initial particles.
- Fracture occurs through rapidly applying intense stresses (impact). The broken particle size distribution in this case will range between 20 and 70 % v/v of the size of the initial particle.

The grinding mechanisms can be studied by comparing the experimental data with the characteristic behavior of the grinding mechanisms as illustrated in Fig. 15.3.

The initial particle size distribution of the material slowly shifts to smaller particle sizes during the first 5 min of grinding. The first breakage events only

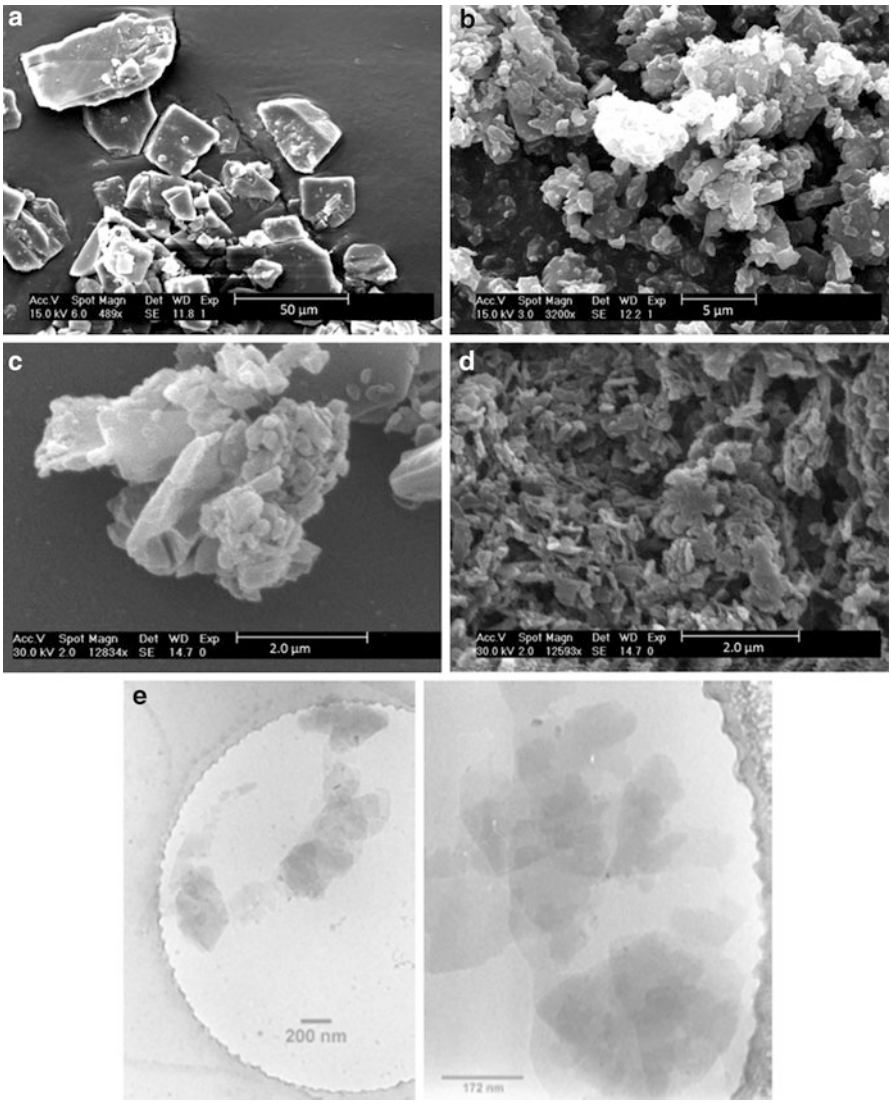

Fig. 15.8 Scanning electron microscopy imaging of particles after different grinding times: (**a**) starting material; (**b**) 10 min grinding; (**c**) 30 min grinding and (**d**) end product after freeze drying—140 min grinding; (**e**) Cryo-TEM picture after 20 min grinding

require a small amount of energy. This breakage leads to only a few daughter particles and therefore cleavage is the dominant grinding mechanism.

In a later stage during grinding, smaller particles appear and the distribution becomes bimodal. The particle size measurements have been complemented with scanning electron microscopy (SEM) pictures taken from samples dried at room temperature at different grinding times. Figure 15.8 shows that the decrease in

Table 15.2 Particle size and grinding time after start of the circuit operation as function of the grinding medium bead size and rotation speed. (time t_Z required to reach the minimum reachable (final) $D_{4,3}$)

		Mean diameter grinding media (mm)		
		0.300	0.500	0.800
		Final mass mean diameter $D_{4,3}$		
		(Time of grinding to final product t_Z)		
Rotation speed (rpm)	2,000	0.181 μm (53 min)	0.173 μm (116 min)	0.175 μm (260 min)
	3,000	0.180 μm (47 min)	0.188 μm (120 min)	0.179 μm (175 min)
	4,500	0.184 μm (29 min)	0.183 μm (69 min)	0.175 μm (145 min)
	6,000	0.177 μm (26 min)	0.183 μm (50 min)	0.176 μm (112 min)

particle size between 5 and 10 min of grinding leads to coarse particles covered by many fine particles. This behavior is typical for the abrasion breakage mechanism.

The formation of intermediate sized particles is observed after circa 30 min of grinding. This broad range of particles shows that the breakage is mainly resulting from a complex breaking process which includes abrasion, cleavage and/or fracture. The SEM image in Fig. 15.8c shows a large amount of fines, intermediate sized particles, coarse particles and agglomerates/aggregates ('clusters'). The presence of fines is characteristic of the abrasion mechanism. It is not easily visible on the picture if the other broken particles are resulting from a cleavage or fracture process. The breakage of intermediate sized particles is mainly resulting from a double breaking process which includes abrasion and cleavage or fracture.

Finally, all intermediate sized particles break down to the final particle size. The difference between those particle sizes is not big and breakage can therefore be classified as a cleavage process. SEM picture (Fig. 15.8d) was made of a freeze dried sample. Small particles appear to be present as clusters but their presence can still be observed.

15.2.5 Milling in Absence of Additives

A stirred media mill is a complex system with many parameters that influence the process of grinding. The more important parameters are rotation speed, grinding medium size hardness and density, filling ratio, product concentration, etc. This study focuses on grinding medium size and rotation speed. The grinding medium used is made of Zirconium oxide stabilized with Yttrium. The sizes of the grinding beads (D_{GM}) are of 0.3, 0.5 and 0.8 mm. The rotation speed ranges from 2,000 to 6,000 rpm. Filling ratio of the mill is 80 %. Considering the size of the impellor blades, the tip speed ranges from 6.8 to 20.4 m/s. The results are presented in Table 15.2.

In all experiments a similar final particle size (about 180 nm) was reached regardless of grinding medium size and rotation speed. The grinding time

was, however, strongly dependent upon both parameters. The model to be developed should therefore allow definition of the time required for grinding as a function of its parameters, which themselves should be defined as a function of the process parameters.

15.2.6 Milling in Presence of Surfactants

The free energy of particles increases with an increase in specific surface area. When particles form agglomerates the total surface area decreases. As a result the free energy is lowered and the system is more stable. Agglomerates are formed when particles overcome the inter-particle energy barrier [33].

The driving forces for agglomeration are Brownian motion and fluid motion. In a stirred media mill the particles can be pressed together between two grinding beads or between grinding beads and the wall of the mill. When particles are pressed together they can agglomerate or aggregate. The resulting clusters can again be broken up into smaller particles in the stirred media mill.

In the final coating application, at a given concentration, clustered particles are more spaced apart from each other than non-clustered particles would be. One objective of grinding is to obtain smaller particles to reduce the distance between them in the coating application. The benefits from grinding would thus not be optimized in a case clustering occurred.

Clustering can be prevented with additives that give electrostatic and/or steric repulsion between the particles. The choice of additives is dependent on the product and its application(s). Griffin [15, 16] and Davies [6] calculated the hydrophilic-lipophilic balance (HLB) number for surfactants on the basis of the molecular weight of the hydrophilic and hydrophobic parts of the molecule. The HLB number helps to make a first selection of a stabilization system.

The grinding experiments from Sect. 15.2.5 were repeated with CTAB (Cetyl-trimetyl-ammonium bromide), a cationic surfactant to stabilize the particle suspension and to prevent agglomeration of small particles. A cationic surfactant is used as the particles have a negative zeta potential in the condition of grinding (pH ~6; Zeta potential in Fig. 15.11). As described for example by Bernhardt [3], the use of an additive will help to prevent broken particles from agglomerating. Therefore the final particle size reachable could be smaller when surfactants are used.

Figure 15.9 shows that an increase in surfactant concentration reduces the mean particle size after grinding. The observed effect is most likely due to stabilization of the particle suspension by the surfactant, which prevents/reduces particle agglomeration. The surfactant was present as micelles at the concentrations that were used (critical micelle concentration CTAB $= 1$ mmol.L^{-1}). These micelles could affect the particle size measurement. As a result a lower average particle size could be measured in the presence of surfactant micelles. The surfactant was added prior to grinding. The surfactant thus might affect all particle size measurements

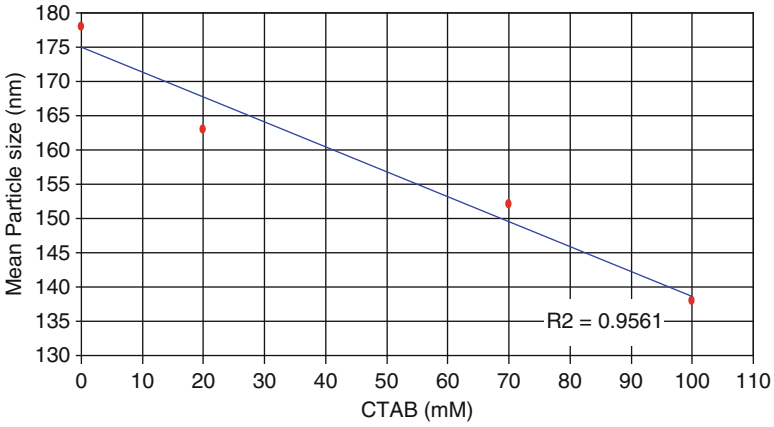

Fig. 15.9 Final particle size in ball milling as function of CTAB surfactant concentration

in one grinding experiment. The particle size before grinding was the same in all experiments regardless of the use of surfactant. It may therefore be concluded that the micelles did not affect the particle size measurement in any of the experiments.

The addition of surfactant can change the solubility and degradation rate of the product and thereby induce a particle size reduction. Solubility could be measured using filtration of dispersed suspensions (0.02 μm filters) and HPLC techniques. Tests were performed to verify if the particle size decrease was related to a solubility increase. For CTAB concentrations of 0 and 100 mmol.L^{-1} the particle size changed from 0.18 to 0.14 μm after grinding, which implies an average single particle mass reduction of 47 %. The concentration of total product in the liquid phase was 0.5 % w/w in all experiments. In absence of surfactants the solubility was limited to 50 ppm. In the presence of surfactants (100 mmol.L^{-1}) the solubility reached 170 ppm. The decrease of total particle mass due to solubilization therefore was 2 % w/w. This is much less than the decrease of 47 % that is observed as the result of grinding. This proves that the surfactant prevents agglomeration of particles.

Another experiment was performed to determine the influence of the surfactant on the product solubility and the particle size analysis. 100 mM CTAB was added to a 180 nm particle suspension that did not contain surfactant. The particle size was measured before and after surfactant addition. Upon the addition of surfactant the particle size decreased from 180 to 170 nm after several hours of magnetic stirring. The decrease in particle size could be related to solubilization or de-agglomeration of the particles. The particle size in presence of surfactant was thus much higher than 140 nm, which was reached when surfactant was added prior to grinding. This confirms that the surfactant had a small effect on the particle size measurement.

15.3 Characterization of Extra Fine Milled Product: Particle Size and Particle Stability

15.3.1 Particle Size Characterization of Extra Fine Milled Product

In this part the particle size distribution of sub micrometer particles suspended in a liquid is described. The particles milled are an organic poorly water soluble crystalline product. To characterize the size of these particles, different techniques have been tested: Imaging techniques (SEM, Cryo-TEM), static light scattering techniques, dynamic light scattering techniques, centrifugation and flow field flow fractionation.

The results indicate that the studied milled particles have a primary particle size close to 180 nm and there is strong evidence of larger particles which are very likely clusters. This is clearly seen from the Cryo-TEM results (Fig. 15.8e).

All the above mentioned techniques should in principle be able to measure samples of dispersion containing particles of ca 180 nm but several are disturbed by the presence of clusters. It is difficult to estimate the amount of cluster present, but most of the time one is interested in what the primary particle size distribution is.

It is clear that no single piece of equipment is capable of exactly determining the particle size distribution of our samples, but the static light scattering with low shear on mixing does give a good representation of what is seen with the image analysis by Cryo-TEM.

In this work frame, it is important to determine the final particle size distribution of the milled particles. This enables the evaluation of the efficiency of the grinding process.

It is also important to evaluate the stability versus aggregation of the milled particles. It has been shown in previous studies that milled particles can quickly aggregate [21, 33]. The presence of aggregated milled particles can be seen as large particles in the particle size distribution.

Several commercially available techniques have been tested. All the tested techniques are capable to analyze sub micrometer particles dispersed in a liquid. For each technique, particles milled and stored at the same conditions have been used. The size distribution has been measured with each sizing technique.

The different techniques available on the market can be drawn together in several groups [17, 31]:

Image analysis techniques
Static light scattering based techniques using:

- Polarization Intensity Differential Scattering (PIDS)
- High resolution CCD detectors
- Blue wave technology
- Backscattering detection

Techniques based on the Brownian motion of the particles. Those techniques uses:

- Photon correlation spectroscopy (PCS)
- Photon Cross Correlation Spectroscopy (PCCS)
- The Heterodyne principle
- Particle Tracking

Centrifugation
Flow field flow fractionation techniques
Other techniques available commercially which are not tested in this work are:

- Particle separation by size exclusion chromatography
- Acoustics and electro-acoustics

The results of the various techniques used to measure the particle size distributions are summarized in Table 15.3.

A detailed description of each technique is presented in the next section.

Image analysis of SEM pictures shows primary particles of around 180–200 nm. The accuracy of the SEM results depends on how representative the sample in the picture is and how many particles are counted. Measuring 100 particles does not pretend to give an accurate result but is an indication of an order of size. The product suspension is dried and gold coated before being introduced in the SEM. Therefore the samples are not systematically representative for the original particles in suspension. The clustered structure could be created during the drying step. An answer to this point is possible using the Cryo-TEM technology.

The sample preparation for the Cryo-TEM imaging includes a process of cryonization that is quick enough (ca 1 ms) to freeze the water in a glassy state and to fix the particles as they are in the suspension. The particles seen in the frozen matrix are thus expected to be in the same as in the suspension. Figure 15.8 shows clearly that the ground particles are clustered. The size of the primary particles corresponds to the size measured by the SEM (0.18–0.20 μm) and the clusters are in the micrometer range. From the Cryo-TEM (Fig 15.8e) analysis it can be concluded that the aggregates are present in suspension. Similar clusters are seen in the SEM pictures as well. Thus, the clustered structures observed in the SEM pictures were probably not created during the drying step but are present in the suspension of ground particles.

Cryo-TEM also shows presence of larger clusters. Several techniques do see the small particles of the same size as well as some larger particles. The size of these larger particles could be measured by some techniques to range mainly between 1 and 50 μm.

Some of the static light scattering instruments show both small and larger particles but the Beckman Coulter LS 13320 and the Horiba LA950 only see the small particles. There is very little difference between the processing of the particles during the size measurement. They are all measured at similar

Table 15.3 Overview of the results given by the different particle size measurement techniques

Technique		Time of measur ement	Mean primary particle size $D_{4,3}$ (nm)	Large particles	Remarks
Imaging techniques	Imaging techniques SEM	1day	194[a]	Yes	The SEM requires drying and therefore aggregates cannot be differentiated from the smaller particles. The technique enables a good evaluation of the shape of the particles
	Imaging techniques Cryo-TEM	20 min	180–200[a]	Yes (2–3 μm)	Cryo-TEM enables an "in solution" look to the particles and enables to see the aggregates and estimate their size as well as the one of the primary particles
Static light scattering	+ PIDS – Beckman coulter LS13320	~ 5 min	181	No	
	High Res. Detect. Saturn DigiSizer 5,200	<5 min	354	Yes (1–10 μm)	
	+ Blue Light Malvern Mastersizer	<5 min	187	Yes (1–50 μm)	
	+ Back scattering Horiba LA950	<5 min	180	No	
Brownian motion based techniques	PCS	~ 10 min	–	"Yes"	No measurement was possible because of the high influence of the concentration and the presence of large particles
	PCCS	~ 5 min	188	Yes (>1 μm)	The light aggregates are detected and are above the detection maximum of the machine (1 μm)
	Heterodyne	~ 5 min	853	Yes	Only the big particles are detected, they most probably disturb the measurement

Particle tracking	~ 5 min	277	No	The few number of particle actually analyzed in the present case do not enable an accurate quantitative analysis. The coarse particles are not detected; they might have sediment before the measurement
Disc Centrifugation	20–30 min	381	No	Streaming effects and high Reynolds number might be responsible of the higher values of the particle size measured. High gravity and drag forces might break aggregates
Flow field flow fractionation	60–90 min	170[b]	Yes	The aggregate particles elute after a very long time. The total distribution could not be therefore detected

[a]average length of particle (not $D_{4,3}$)
[b]median particle size

concentrations and all in demineralized water without surfactant. All samples are pumped through the measurement cell by using a centrifugal pump. Slight differences are seen in the design of this pump and the shear induced on the product. Should the Horiba LA 950 and the Beckman Coulter LS13320 devices induce higher shear on the clustered particles than the Malvern Mastersizer, those clusters might break in these first two instruments and remain intact in the Mastersizer. Differences might also be due to the de-convolution procedure or to filtering of the data when small amounts of larger particles are detected.

The Digisizer shows larger particles than the other instruments based on static light scattering. Note that the measured scattering pattern includes signals of both primary particles and clusters. The resulting scattering pattern is therefore very complex. The CCD detectors are capable to detect that scattering pattern at higher resolution but not all acquired data can be processed because of lack of data processing power. That inaccuracy in the calculation might explain the difference in the particle size measured. No quantification of the error made on the value of the particle size could be made to confirm this hypothesis.

Dynamic light scattering techniques are difficult to use because they are strongly influenced by the presence of larger particles. When they settle they give rise to a high motion which results in a shift of the particle size distribution.

Only photon cross-correlation spectroscopy shows about the same primary particle size as the image analysis. In addition the particle size distribution indicates that larger particles may be present. But their size cannot be obtained, because the upper limit of detection is around 1 μm.

Since the sample is neither stirred nor undergoing any shear, clusters would not be broken. The large particles observed are thus most probably the clusters observed on the Cryo-TEM and SEM pictures. No measurement can be done while stirring or applying shear. That would induce a movement of the product particles in addition to Brownian motion, and the measurement results would be wrong.

The measurement in the case using the heterodyne technique is not reliable enough to clearly determine the cluster size. Nevertheless, the presence of large particles is clear. Larger particles move because of sedimentation and not only Brownian motion. The signal emitted by big particles is influencing the correlation function a lot. The fitting of the correlation function is extremely sensitive and results in huge differences in the obtained particle size distributions.

The mean volume-based particle diameter $D_{4,3}$ obtained using particle tracking technique is 277 nm, which is in the order of magnitude as the results given by image analysis and static light scattering techniques.

No coarse particles are detected; it is possible that the coarse particle sediment out from the focal plane before or during the measurement. They would then not be analyzed.

Centrifugal sedimentation is capable to see smaller particles but larger particles are expected to sediment that fast that they are not detectable. The

mean particle size measured is 381 nm; slightly bigger than the one observed by image analysis (180–200 nm) but the results remain in the order of magnitude [30]. Two aspects can be responsible for a larger mean particle size as expected (Laidlaw and Steinmetz):

(a) At the beginning of the analysis, the entire sample is contained in a thin fluid layer near the surface. A streaming phenomenon enables the particles to sediment faster which leads to a broad initial band. The sedimentation follows then a normal pattern but the calculation of the particle size from the slightly shorter sedimentation time would give slightly bigger results of the particle size.
(b) At very high rotation speed as in the present case (24,000 rpm, ca 2,900 G), the Reynolds number of the particle flow becomes higher and the Stokes law does not describe the sedimentation process accurately. That error could induce a bigger particle size than expected.

Flow field flow fractionation shows primary particles of 170 nm. The results are similar to the results by image analysis. The particle size as detected by a multiple angle scattering device shows a wide distribution. It is not possible from the data to determine the exact particle size distribution of the tested product, a.o. because the elution was not totally finished and no calibration was executed with a reference material. Larger particles are detected by the UV detector but the time of analysis is then very long.

15.3.2 Stability of Particle Suspension After Fine Grinding

The physical stability of sub-micrometer particle suspensions of organic crystalline food compounds after grinding will be described next. A Dynomill ball mill was used in combination with zirconium oxide grinding beads. The organic product was a poorly water soluble product. During grinding the average particle size of the particulate product was reduced to a minimum value in the sub-micrometer range. Forward light scattering was used to analyze the particle size distribution. Dynamic light scattering measurements, on the other hand, showed that clusters were present after grinding. The difference in the obtained particle size distributions using both techniques was related to the shear in the measurement device, i.e. in the laser diffraction measurement the shear was higher than in the dynamic light scattering device. Thus in the laser diffraction measurement the clusters were broken up by shear, while this was not the case in the dynamic light scattering measurements. The difference in the measurements showed that the particles formed clusters at low to zero shear.

The clustering of the particles was studied by measuring the sedimentation behavior of the particles suspension at various pH values. The impact of the pH on the clustering rate can be explained by the zeta-potential of the particles.

Sedimentation Measurements

Freshly ground particle suspensions (1.0 % solution with 0.01 mol.L^{-1} NaCl) were divided over several bottles. The pH was adjusted to values between 3 and 9 using sodium hydroxide (0.01 mol.L^{-1}) and hydrogen chloride (0.01 mol.L^{-1}). The ionic strength was thus constant at all pH values. At pH 10, to be able to reach the right pH, the ion concentration was increased to 0.05 mol.L^{-1}. The amount of acid and base that was required was low compared to the sample volume. The dilution was thus negligible. The pH was set over a period of 48 h by incremental acid or base dosage until the desired pH was reached. During the process the samples were continuously stirred. After pH adjustment the samples were put in graduated pipettes of 10 mL that were closed with a rubber stop to avoid evaporation of liquid. The sedimentation front was recorded over a period of 15 days.

Zeta Potential Measurements

The measurements were carried out with freshly prepared suspensions of ground particles. These suspensions were diluted to 0.1 % prior to measurement in the ZetaSizer (Malvern, UK). The ionic strength was fixed to 1 mM using potassium chloride. The zeta potential was determined as function of pH by automatic titration from pH 3 to 10 using a 4 N sodium hydroxide solution.

Sedimentation Tests

The sedimentation data is presented in Fig. 15.10. The initial sedimentation velocity can be used to determine the cluster size at t = 0, i.e. directly after mixing and setting the pH. Particle sedimentation in these experiments occurred under laminar flow, because the Reynolds number for particle sedimentation was very low in all cases. The suspensions contained 0.76 % v/v of organic particles. It is expected that this concentration is low enough to avoid swarm effects in sedimentation. The sedimentation rate of particle swarms is defined by the Richardson-Zaki equation [7, 28]:

$$v_{swarm} = v_s \cdot {c_V}^n \tag{15.1}$$

where v_{swarm} is the sedimentation rate of a swarm, v_s the settling rate of one particle, c_V the volume fraction liquid ($c_V = 99.24$ %), n is a factor dependent on the Reynolds number (Re < 0.2 in any case), and can be calculated by:

$$n = 4.6 + 20 \cdot \frac{D_p}{D_v} \tag{15.2}$$

where the particle diameter being D_p ($D_p = 1.64$ μm in the worse case) and the vessel diameter being D_v (1.0 cm).

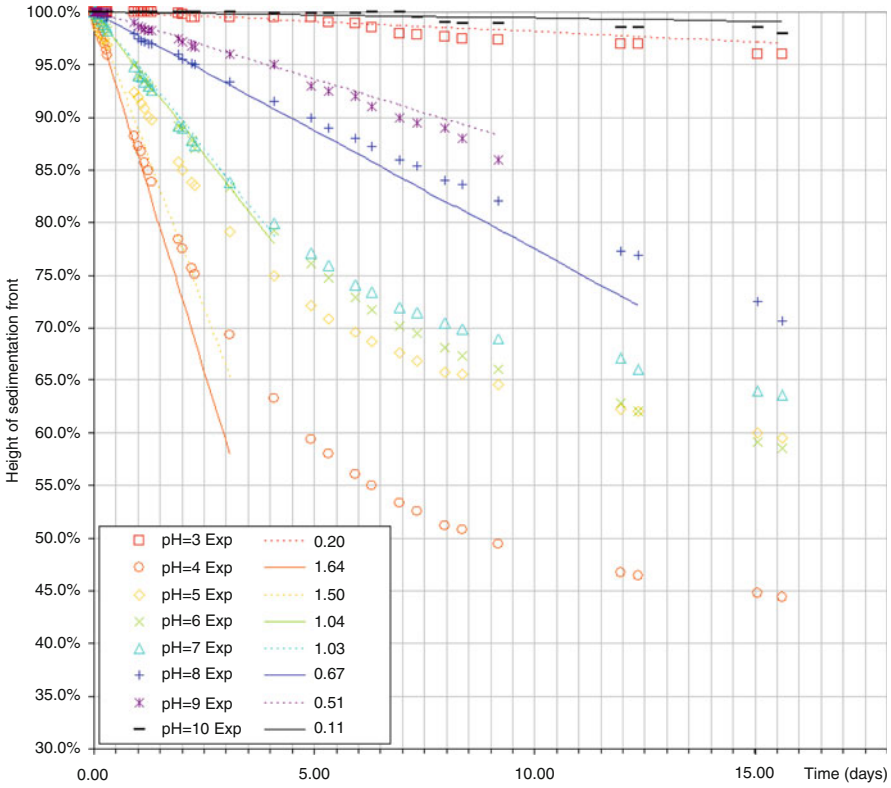

Fig. 15.10 Sedimentation profile of ground particles as function of pH. Symbols relate to experimental values, lines to fitting of Stokes sedimentation theory with indicated cluster size (in μm)

For the system that is considered in this work $n = 4.60$ and the swarm speed is 97 % of the settling velocity of the single particles. This confirms that swam effects are negligible in this work. The settling velocity of the particles can thus be expressed by Stokes law:

$$v_s = \frac{\left(\rho_p - \rho_f\right) \cdot D_s^2 \cdot g}{18 \cdot \eta_f} \tag{15.3}$$

with η_f is the fluid viscosity, D_s the Stokes particle diameter, ρ_f the fluid density (1,000 kg/m^3), ρ_p the particle density and g is the gravitational acceleration. The particle density was measured by sucrose gradient centrifugation [32]. This density was approx. 1,300 kg/m^3.

Figure 15.10 depicts sedimentation data and fits of the initial sedimentation rates with Stokes law. The graph shows that extreme pH values give higher suspension stability than intermediate pH values. This observation can be explained by the zeta

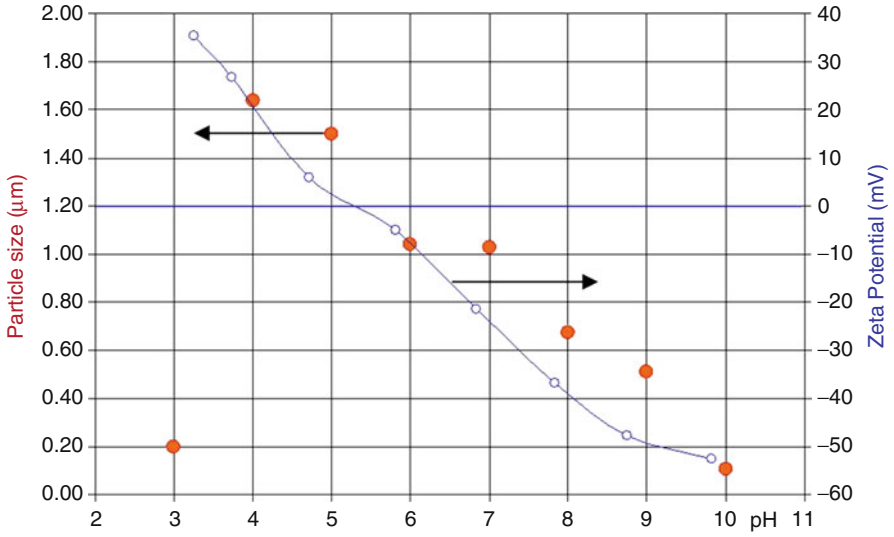

Fig. 15.11 Zeta-potential (*line*) and calculated Stokes equivalent particle size (*dots*) as function of applied pH

potential measurements that are presented in Fig. 15.11. The particle size determined by sedimentation measurements corresponds reasonably well to the Cryo-TEM picture in case of unstable suspensions, i.e. highest sedimentation rates. The particle size determined by sedimentation measurements in case of stable suspension, i.e. lowest sedimentation rate, corresponds reasonably well to the forward light scattering measurements.

The iso-electric point of the ground organic product particles is approx. 5.3. The degree of agglomeration increases when the pH approaches the iso-electric point, which can be explained by the reduction in the electrostatic repulsion between the particles.

At pH 4 the sedimentation seems to be higher than at pH 5 or 6. This is contradictory to the expectation on the basis of the zeta-potential measurements. This contradiction can be explained on the basis of the experimental protocol. The pH of the particle suspensions was set during a period of 48 h. The pH after grinding was 5.7. The iso-electric point was thus passed for suspensions with a pH below 5.7. The stability during pH control was thus different for samples above pH 5.7 and below pH 5.7. The clusters that were formed during pH control could be broken up at different rates depending on the zeta-potential and the applied shear. The shear was constant in all cases. It is therefore expected that cluster break up rate during pH control was higher for more extreme zeta potentials.

An alternative approach would have been to grind the product at the desired pH values instead of setting the pH after grinding in order to avoid passing the iso-electric point for stability testing. Grinding experiment were carried out at various pH values for the study of the grinding mechanism. It was shown that the grinding kinetics are independent of pH.

15.4 Distribution of Poorly Soluble Particles in Films and Coatings

In Sect. 15.2, sub-micrometer particles are produced. In Sect. 15.3, the particles are characterized and there stability investigated. In this part, the ground particles are applied in an example of food stuff: a cheese coating.

Several research groups in the food industry have been studying antimicrobial agents in food and on food surfaces (among others [13, 36–38, 43, 46, 47]). The aim of these studies was to obtain optimal antimicrobial protection of the food stuff. In all the cited papers it is highlighted that the shelf life is systematically dependent upon an optimum balance between:

1. The molecular diffusivity of the ingredient
2. The consumption or degradation rate of antimicrobial ingredient
3. The dissolution behavior
4. The homogeneity of the distribution of the particles of the antimicrobial compound.
5. The minimum inhibitory concentration (MIC) of the antimicrobial compound. Microorganisms are able to grow in or on the food stuff when the concentration of the antimicrobial compound in or at the surface of the food stuff is below the MIC. The microbial shelf life of the food stuff is thus limited by the time the dissolved preservative concentration remains above the MIC.

Optimization of the microbial shelf life of the coated food stuff requires a study on the interaction between all five parameters that were mentioned above. Diffusivity depends amongst others on the nature of the matrix, temperature, and the size of the antimicrobial compound. Increasing the diffusivity enables a better coverage of the food stuff and may thus lead to an increase of the microbial shelf life of the food stuff when diffusion of the preservative is limiting [10, 12, 29, 39]. Consumption and/or degradation of the preservative are dependent upon the chemical stability and the presence of microorganisms that are attacked by the antimicrobial compound. Dissolution of the preservative particles depends on the properties of the particles and the surrounding medium and the available surface area for dissolution. The preservative particle distribution is dependent on the preservative dosage and particle size. The critical dissolved concentration of the preservative is given by the MIC for the microorganisms from which the food stuff needs to be protected.

In this section the objective is to determine the influence of the preservative particle size on the shelf life of the coated food stuff. In a first step, a model is used to evaluate the impact of the above mentioned parameters. All aspects of the model (diffusion, degradation, dissolution and distribution) are presented before a theoretical model is calculated. In a second part the experimental method for the determination of each aspect is presented. Finally, the experimental results are given and an accelerated shelf life test is used to experimentally verify the model calculations.

Different sizes of the preservative particles were obtained by wet grinding. Particle sizes of 15 μm and approx. 0.2 μm were tested.

15.4.1 Modeling of the Distribution of Particles and Diffusion of Preservative Molecules in a Coating

The MIC for the microorganisms is assumed to be constant at one third of the solubility of the preservative, C_S. The shelf life t_c of the coated food stuff is reached when the preservative concentration at the weakest location in the coating is below the MIC. The weakest location in the coating is the farthest point from the preservative particles. The distance between two particles is δ. The farthest point between the two particles is thus $\delta/2$. The shelf life t_c of the coated food stuff is thus resembled by Eq. 15.4:

$$C\left(\frac{\delta}{2}, t_c\right) = \frac{C_S}{3} \tag{15.4}$$

The concentration C of preservative molecules is defined by Fick's [8, 9] second law of diffusion and a degradation term $B(x,t)$.

$$\frac{\partial C(x,t)}{\partial t} = \mathbb{D} \cdot \frac{\partial^2 C(x,t)}{\partial x^2} + B(x,t) \tag{15.5}$$

where C is the dissolved preservative concentration (ppm), x the position between two preservative particles (m), t the time (s), $\mathbb{D}$ the diffusion coefficient ($m^2.s^{-1}$).

Diffusion The diffusion coefficient $\mathbb{D}$ for a molecule can be described by Eq. 15.6.

$$\mathbb{D} = \frac{k \cdot T}{3 \cdot \pi \cdot \eta_f \cdot d_m} \tag{15.6}$$

where k is the Boltzmann constant, d_m the diameter of the molecule assuming a spherical molecule, η_f the fluid (or matrix) viscosity and T the temperature. The apparent diffusivity will be lower when the molecule is not spherical [40]. The characteristic time for diffusion (τ_{diff}) is defined as the time required for a molecule to diffuse over the distance δ (Eq. 15.7):

$$\tau_{diff} = \frac{\delta^2}{\mathbb{D}} \tag{15.7}$$

Dissolution and solubility The dissolved preservative concentration directly after application of the coating to the food stuff is assumed to be equal to the

solubility (C_S) of the preservative. This is the starting point for the model calculations, i.e. $C(x,0) = C_S$. The second assumption for the model calculations is that the concentration of dissolved preservative at the preservative particle surface is equal to the solubility of the preservative, i.e. the dissolution rate is much faster than the diffusion and degradation rates. The boundary condition for the model calculations thus is: $C(0,t) = C_S$ and $C(\delta,t) = C_S$. The validity of these assumptions will be proven further on in this chapter (Sect. 15.4.3).

The dissolution rate constant (k_{diss}) for the preservative is defined from Noyes and Whitney [35] as:

$$\frac{dC(t)}{dt} = k_{diss} \cdot (C_S - C(t)) \tag{15.8}$$

With $C(t)$ the concentration of the preservative in time and C_S the product solubility.

The value of k_{diss}, degradation rate constant (only the dissolved material will degrade, not the solid material present), was determined in the coating prior to application at room temperature in absence of light. The preservative concentration was measured as function of the storage time. The initial preservative concentration was 6.5 times the value of the solubility C_S. First order degradation reaction kinetics (Eq. 15.8 with n = 1) were fitted to the experimental data.

In application the preservative-containing coating will be exposed to another environment. The preservative will undergo more potential degradation mechanisms such as oxidation due to contact with air and higher microbial contamination which may lead to enhanced consumption of the preservative. The degradation rate constant that has been measured in this work is thus expected to be an underestimation of the degradation rate constant that can be encountered in application.

From the fit of the experimental data using Eq. 15.8 $k_{diss} = 0{,}95\ s^{-1}$ was obtained for 0.2 μm particles. For 15 μm particles this was $0.05\ s^{-1}$.

The characteristic time for the preservative dissolution process (τ_{diss}) is inversely proportional to the dissolution rate constant k_{diss}.

$$\tau_{diss} = \frac{1}{k_{diss}} \tag{15.9}$$

Distribution: The shelf life of the coated food stuff is assumed to be equal to the time that is required to reach the MIC for the dissolved preservative at any position in the coating. The most critical point in this respect is the position in the coating where the distance between the preservative particles is the largest. At this position the distance that needs to be traveled by the dissolved preservative molecules from the preservative particle surface, where dissolution takes place, to a position in the middle between two preservative particles is the largest. The biggest gaps in the coating with regard to preservative particle coverage are thus most critical for the shelf life of the coated food stuff.

The determination of this critical gap size in the preservative particle coverage is discussed in Sect. 15.4.3, results are given in Sect. 15.4.4.

Equation 15.5 becomes thus Eq. 15.10:

$$\frac{\partial C(x,t)}{\partial t} = \mathbb{D} \cdot \frac{\partial^2 C(x,t)}{\partial x^2} - k_d \cdot C(x,t) \tag{15.10}$$

The initial (IC) and boundary (BC) conditions as described above are:

$$\begin{cases} IC : C(x,0) = C_s \\ BC : C(0,t) = C(\delta,t) = C_s \end{cases} \tag{15.11}$$

With C_S being the solubility of the product in the matrix.

The model has been analytically solved using a Fourier series. Equation 15.12 shows the solution of Eq. 15.10 using the initial and boundary conditions:

$$C(x,t) = C_s + \sum_{n=0}^{\infty} \frac{4 \cdot k_d \cdot \delta^2 \cdot C_s}{\mathbb{D} \cdot ((2 \cdot n + 1) \cdot \pi)^3 + (2 \cdot n + 1) \cdot \pi \cdot k_d \cdot \delta^2} \cdot \left(e^{-\left(\mathbb{D} \cdot \left(\frac{(2 \cdot n + 1) \cdot \pi}{\delta} \right)^2 + k_d \right) \cdot t} - 1 \right) \sin\left(\frac{(2 \cdot n + 1) \cdot \pi \cdot x}{\delta} \right) \tag{15.12}$$

Equation 15.12 is valid until the preservative particles are fully dissolved in the coating matrix. At the time noted $t_{\varnothing}$ the preservative particles are fully dissolved and the boundary conditions change into $BC_{\varnothing}$:

$$BC_{\varnothing} : \left.\frac{\partial C(x,t)}{\partial x}\right|_{x=0} = \left.\frac{\partial C(x,t)}{\partial x}\right|_{x=\delta} = -k_d \cdot C(x,t) \tag{15.13}$$

The time $t_{\varnothing}$ at which the preservative particles are fully dissolved is given by Eq. 15.14:

$$m_{part}\Big|_{t=0} = \mathbb{D} \cdot s_{part} \cdot \int_{t=0}^{t_{\varnothing}} \left.\frac{\partial C(x,t)}{\partial x}\right|_{x=0} .dt \tag{15.14}$$

With $\left.\frac{\partial C(x,t)}{\partial x}\right|_{x=0}$ being the flux of product from the particle surface into solution, m_{part} being the mass of the particle and S_{part} the surface of the product particle.

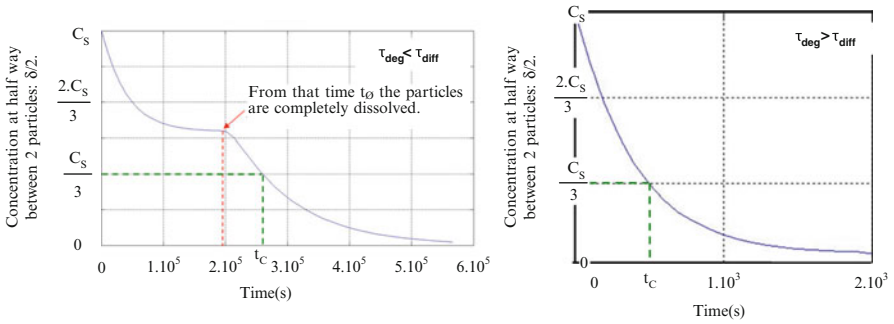

Fig. 15.12 Concentration profile of active product at equal distance between two particles: $C(\delta/2, t)$ *Top*: The shelf life is reached after the preservative particles are fully dissolved ($t_C > t_{\emptyset}$). *Bottom*: The shelf life is reached before the preservative particles are fully dissolved ($t_C < t_{\emptyset}$)

Numerical calculations were performed in Matlab.

The critical time was determined for a range of values of the characteristic times of diffusion (τ_{diff}) and degradation (τ_{deg}). The characteristic time for dissolution was assumed to be much smaller than the characteristic times for degradation and diffusion.

An example of the concentration profiles of the preservative at $\delta/2$ is given in Fig. 15.12 for conditions when diffusion is faster than degradation and vice versa. As illustrated, the initial concentration at $t = 0$ is the product solubility C_S. The concentration decreases in time because of the degradation process that is partly compensated by the diffusion from the product particle. The graph shows that when the particles are completely dissolved, at $t = t_{\emptyset}$, only degradation takes place and a second drop in concentration is observed. The critical time (the shelf life t_C) is reached when the concentration at $\delta/2$ is of one third of the product solubility C_S. When the characteristic diffusion time for degradation is higher than the characteristic time for diffusion ($\tau_{deg} > \tau_{diff}$) then $t_C > t_{\emptyset}$, and vice versa.

The numerical calculations show that a small characteristic diffusion time and a high characteristic degradation time are the best for a long shelf life, which is logical because under these conditions diffusion of dissolved preservative molecules is much faster than degradation of dissolved preservative molecules. Under these conditions the diffusion process is fast enough to supply preservative throughout the coating without degradation causing local dips in the dissolved preservative concentration. The opposite, a short characteristic degradation time and a long characteristic diffusion time, gives a short shelf life because the diffusion process is not fast enough to allow for rapid replacement of degraded preservative in the coating.

15.4.2 Characterization of the Distribution of the Particles in the Matrix

Inhomogeneities in the preservative particle distribution are seen as a Normal and broad distribution of particles in the matrix. Those inhomogeneities are unfavorable

for the shelf life of the coated food stuff because inhomogeneities result in larger inter-particle distances locally in the coating matrix. An increase in inter-particle distance gives an increase in the diffusion distance and thus shifts the balance between the diffusion rate and the degradation rate in favor of the degradation rate. The process of dispersing the particles in the matrix should thus be optimized to achieve a homogeneous preservative particle distribution. In the present case study the particles were well mixed throughout the coating matrix. The coating was applied by dipping the food stuff into the coating. The applied coating was dried at ambient conditions. This procedure is expected to give a random distribution of the preservative particles in the applied coating.

15.4.3 Calculation of the Inter-Particle Distance Distribution

In Fig. 15.1 the preservative particles are projected onto a 2D surface. Assuming a random particle distribution in the coating matrix, the distribution of squares that do not contain any preservative particles can be calculated analytically using the Bose-Einstein statistics. The number of empty squares M_{empty} is calculated as function of the total number of squares M and the number of particles N according to the following equation:

$$M_{empty} = \frac{M \cdot (M-1)}{M+N-1} \tag{15.15}$$

The probability P that a square surface area is empty is equal to the fraction of empty squares:

$$P = \frac{M_{empty}}{M} = \frac{(M-1)}{M+N-1} \tag{15.16}$$

Equation 15.16 gives the probability distribution for the empty square size. Given a confidence interval (probability P) and a concentration (number of particles N), the value of the number of cells (M) can be calculated (Eq. 15.16). The surface area of a cell is calculated as the ratio between the surface area of coating and the corresponding number of cells (M) (Eq. 15.17):

$$Surface\ of\ 1\ cell = \frac{1}{M} = \frac{1}{\frac{P}{1-P} \cdot N_{part} + 1} \tag{15.17}$$

The inter-particle distance distribution δ_p is taken as the diagonal size of the empty squares and can be calculated for a given confidence interval P (Eq. 15.18).

$$\delta_p = \sqrt{2} \cdot \sqrt{\frac{1}{\frac{P}{1-P} \cdot N_{part} + 1}} \tag{15.18}$$

With P being the confidence interval ($P = 0.90$ corresponds to δ_{90}, which indicates that 90 % of the empty squares are smaller than the given value) and N_{part} being the number of product particles per unit surface area. The number of particles per unit surface area is calculated from the preservative concentration, the coating thickness and the preservative particle size.

15.4.4 Accelerated Shelf Life Test; Determination of Antimicrobial Activity of the Coating

Freshly brined Gouda cheeses were challenged with Penicillium discolor and coated with various coating formulations to determine the relation between shelf life and coating formulation. Coatings with various preservative particle sizes were applied. The methods that were used to obtain these preservative particle sizes are reported by Van Hee et al. [20]. The number of mould spores that was able to germinate on the treated cheese surfaces is indicative for the anti-fungal activity of the preservative in the coating. The cheeses (10 per coating type) were considered to be no longer protected by the product when 50 % of the cheeses analyzed had at least one growing colony on their surface.

Plasticoat (DSM Food Specialties, The Netherlands) was used as a coating. Several preservative concentrations with various particle sizes were added to this coating. The cheeses were contaminated with Penicillium discolor PED1, CR1A and Penicillium discolor PED74, L1 spores at a concentration of 1.1×10^3 cm^2 after application of the coating. The cheeses were visually checked for fungal growth on a daily basis for 3 weeks. The experiment was carried out with two different preservative particle sizes ($D_{4,3}$), i.e. 15 μm and 0.2 μm

The rate of dissolution is an important aspect. The characteristic dissolution time (τ_{diss}) is much smaller than the characteristic diffusion time (τ_{diff}) and the characteristic degradation time (τ_{deg}).

The model is accurate if the inter-particle distance is at least 10 times larger than the particle size x_i. Fig. 15.13 can be used to determine when this is the case:

For 15 μm particle $\delta_{50} > 150$ μm $\rightarrow C_T/C_S < 70$
For 15 μm particle $\delta_{90} > 150$ μm $\rightarrow C_T/C_S < 700$
For 0.2 μm particle $\delta_{50} > 2$ μm $\rightarrow C_T/C_S < 2$
For 0.2 μm particle $\delta_{90} > 2$ μm $\rightarrow C_T/C_S < 9$

The model as plotted in Fig. 15.14 will be valid in case the concentrations considered are above the limits calculated. The corresponding τ_{diff} can be calculated with Eq. 15.17.

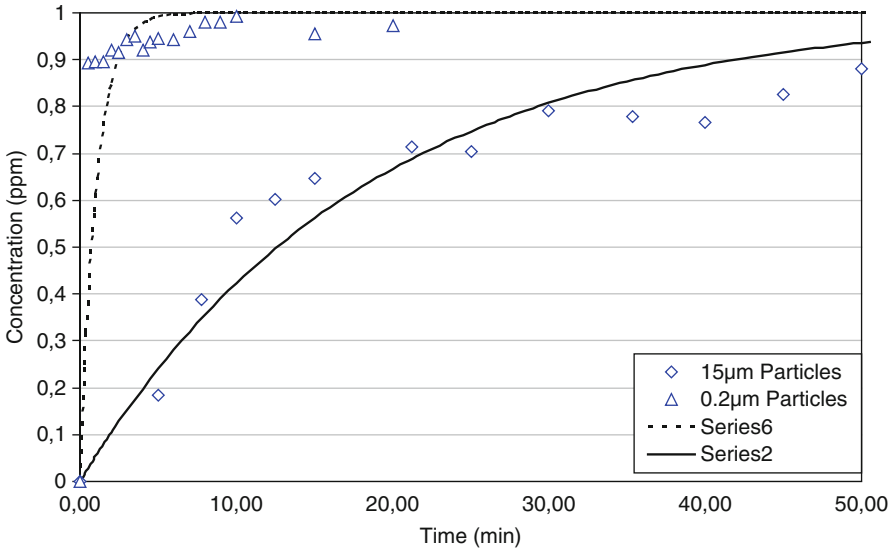

Fig. 15.13 Concentration of dissolved preservative in water as function of time (data points represent measurement data and lines are fits)

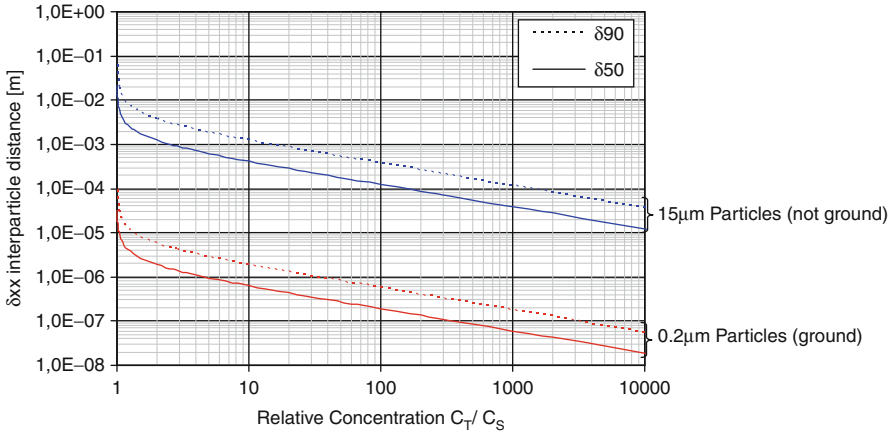

Fig. 15.14 The inter-particle distance distribution (δ_{50} and δ_{90}) for random distributed particles in a matrix as function of the total particle concentration C_T (coating thickness 10^{-4} m)

15.4.5 Experimental Results of the Accelerated Shelf Life Test

Ten cheeses were tested per preservative particle size. As a reference a coating without preservative was tested. The results are presented in Table 15.4.

Table 15.4 Microbial shelf life of coated cheese (the time indicates when 50 % of the cheeses had at least one mould colony; the standard deviation indicates the measurement variation for each set of 10 cheeses)

	Product relative concentration (C_T/C_S)			
Particle size	0.0	3.0	5.0	8.3
15 μm	4 days	–	10.7 ± 2.1 days	11.3 ± 3.0 days
0.2 μm		19.6 ± 4.5 days	20.1 ± 9.6 days	–

The results show that the protection against fungal growth increases when the preservative concentration is increased and/or smaller preservative particles are used.

15.4.6 Conclusions with Comparison of Model and Experimental Results

Model calculations on the distribution of a preservative in a coating were used to determine the microbial shelf life of a coated food product. A case study was performed with a cheese coating containing an anti-fungal compound with low solubility. The preservative was dosed to the coating at concentrations above its saturation concentration. Preservative particles were thus dispersed in the coating. The anti-fungal compound is active only in dissolved state. The dissolution, diffusion and degradation behavior of the anti-fungal compound thus affect the anti-microbial protection that is given by the coating. In addition, the inter-particle distance is of importance. The weakest points in the coating are in the middle between the preservative particles.

The model has shown that an optimum shelf life can be obtained when the characteristic time for diffusion is much shorter than the characteristic time for degradation. The characteristic time for diffusion can be controlled by optimizing the inter-particle distance, i.e. a reduction of the inter-particle distance gives a reduction of the characteristic time for diffusion. At constant preservative concentration the inter-particle distance can be reduced by reduction of the preservative particle size.

The impact of the preservative concentration decreases dramatically when the characteristic time for diffusion is much larger than the characteristic time for degradation. This is due to the fact that the diffusion process is too slow to replenish the degraded preservative in between the preservative particles. Under these conditions the shelf life is mainly determined by the dissolved preservative concentration at $t = 0$ and preservative particles will be present in the coating when the shelf life is reached. This implies that the preservative is not used very efficiently, because not all the preservative that is present in the coating is used for the anti-microbial action of the coating.

Experimental results show that the microbial shelf life of coated cheeses increases with an increase in preservative concentration and/or with a reduction in preservative particle size at constant preservative dosage. These findings correspond to the model calculations. Thus the model gives a reasonable prediction of the accelerated shelf life test. The model shows that the distribution of the preservative particles throughout the coating is of great importance. Such a model can be used to find the optimum formulation for food coatings including the optimum particle size and concentration of active ingredient.

15.5 Definitions, Abbreviations and Symbols

Cluster	Agglomerate and/or aggregate of primary particles
Primary particle	Basic particle that cannot be separated other than by breakage
CTAB	Cetyl-trimethyl-ammonium bromide
PSD	Particle size distribution
SEM	Scanning electron microscopy
TEM	Transmission electron microscopy
$B(x,t)$	Birth/death term [ppm.s^{-1}]
$C(x,t)$	Concentration of product [ppm]
C_S	Solubility of product particles [ppm]
d_m	Diameter of a molecule [m]
d_{50}	Median particle size
$D_{4,3}$	Volume-weighted mean size, mean value of a volume-based PSD
D_p	Particle size
D_v	Vessel diameter
$\mathbb{D}$	Diffusion coefficient or diffusivity [m^2.s^{-1}]
k	Boltzmann constant [m^2.kg.s^{-2}.K^{-1}]
k_{degr}	Constant of degradation [first order: s^{-1}]
k_{diss}	Constant of dissolution [first order: s^{-1}]
m_{part}	Mass of one particles [kg]
$N_{particles}$	Number of particles [-]
S_{part}	Surface area of a particle [m^2]
t	Time [s]
t_C	Microbial shelf life of coated food stuff [s]
$t_\emptyset$	Time at which particles are dissolved [s]
T	Temperature [K]
$V_{suspen.}$	Volume of suspension in the system [m^3]
x	Position [m]
x_i	Particle size [m]
α	Proportionality factor [m.s^{-1}]
δ	Distance between two particles [m]
η_f	Fluid viscosity [Pa.s]
τ_{diff}	Characteristic time of diffusion [s]
τ_{deg}	Characteristic time of degradation [s]
τ_{diss}	Characteristic time of dissolution [s]

References

1. Becker, M., Schwedes, J.: Comminution of ceramics in stirred media mills and wear of grinding beads. Powder Technol. **105**, 374–381 (1999)
2. Bel, F.H., Frances, C., Mamourian, A.: Investigations on ultra-fine grinding of titanium dioxide in a stirred media mill. Powder Technol. **105**(1–3), 362–373 (1999)
3. Bernhardt, C., Reinsch, E., Husemann, K.: The influence of suspension properties on ultra-fine grinding in stirred ball mills. Powder Technol. **105**(1–3), 357–361 (1999)
4. Bilgili, E., Hamey, R., Scarlett, B.: Nano-milling of pigment agglomerates using a wet stirred media mill: Elucidation of the kinetics and breakage mechanisms. Chem. Eng. Sci. **61**(1), 149–157 (2006)
5. Breitung-Faes, S., Kwade, A.: Nano particle production in high-power density mills. Chem. Eng. Res. Design. **86**, 390–394 (2008)
6. Davies J.T.: A quantitative kinetic theory of emulsion type, I. Physical chemistry of the emulsifying agent, Gas/Liquid and Liquid/Liquid Interface; Proceedings of International Congress Surface Activity, pp. 426–438 (1957)
7. Davies, L., Dollimore, D., Sharp, J.H.: Sedimentation of supsensions: Implications of theories of hindered settling. Powder Technol. **13**, 123–132 (1975)
8. Fick, A.: Poggendorff's annal. Physik **94**, 59 (1855)
9. Fick, A.: Phil. Mag. **10**, 30 (1855)
10. Fox, J.B.: Diffusion of chloride, nitrite, and nitrate in beef and pork. J. Food Sci. **45**(860), 1740–1744 (1980)
11. Gao, M., Forssberg, E.: Prediction of product size distributions for a stirred ball mill. Powder Technol. **84**(2), 101–106 (1985)
12. Gennadios, A., Weller, C.L., Testin, R.F.: Temperature effect on oxygen permeability of edible protein-based film. J. Food Sci. **58**, 212–219 (1993)
13. Gill, C.O.: A review, intrinsic bacteria in meat. J. Appl. Bacteriol. **47**, 367–378 (1979)
14. Gontard, N., Guilbert, S., Cuq, J.: Edible wheat gluten film: Influence of the main process variables on film properties using response surface methodology. J. Food Sci. **57**, 190–199 (1992)
15. Griffin, W.C.: Classification of surface-active agents by 'HLB'. J. Soc. Cosmetic Chem. **1**, 311 (1949)
16. Griffin, W.C.: Calculation of HLB values of non-ionic surfactants. J. Soc. Cosmet. Chem. **5**, 259 (1954)
17. Grubenmann, A.: Particle size distribution and aspect ratio of organic pigments. Part. Part. Syst. Charact. **3**(4), 179–186 (1986)
18. Gustavsson, J., Cederberg, C., Sonesson, U., van Otterdijk, R., Meybeck, A.: Global food losses and food waste. Study conducted for the Internat. Congress at Interpack Düsseldorf, Germany Published by the FAO. (http://www.fao.org/docrep/014/mb060e/mb060e00.pdf) (2011)
19. He, M., Wang, Y., Forssberg, E.: Parameter effects on wet ultrafine grinding of limestone through slurry rheology in a stirred media mill. Powder Technol. **161**, 10–21 (2006)
20. Hee, P. Van, Meesters, G.M.H., Wildeboer, W.J., Hennart, S.L.A, Vis, A.J.: Stabilized micronized particles; WO Patent # 2008/110626
21. Hennart, S.L.A., Wildeboer, W.J., Meesters, G.M.H.: Study of the process of stirred ball milling of poorly water soluble organic products using factorial design. Powder Technol. **198**(1), 56–60 (2009)
22. Herbst, J.A., Sepulveda, J.L.: Fundamentals of fine and ultra-fine grinding in a stirred ball mill. International Powder and Bulk Solids Handling Conference, Chicago, pp. 452–470 (1978)
23. Horter, D., Dressman, J.B.: Influence of physicochemical properties on dissolution of drugs in the gastrointestinal tract. Ad. Drug Deliv. Rev. **46**, 75–87 (2001)

24. Hou, T.-H., Su, C.-H., Liu, W.-L.: Parameters optimization of a nano-particle wet milling process using the taguchi method, response surface method and genetic algorithm. Powder Technol. **173**, 153–162 (2007)
25. Howorth, C.J., Lee, W.E., Rainforth, W.M., Messer, P.F.: Contamination rates from Ce and Y-TZP ball milling media. Br. Ceram. Trans. J. **90**, 18–21 (1990)
26. Hu, J., Johnston, K.P., Williams, R.O.: Nanoparticles engineering process for enhancing the dissolution rates of poorly water soluble drugs. Drug Devel. Ind. Pharm **30**(3), 233–245 (2004)
27. Jankovic, A.: Variables affecting the fine grinding of minerals using stirred mills. Minerals Eng. **16**, 337–345 (2003)
28. Janssen, L., Warmoeskerken, M.: Transport Phenomena Data Companion. Edward Arnold Ltd, London (1987). ISBN 0-7131-3618-9
29. Kärger, J., Grinberg, F., Heitjans, P.: Diffusion Fundamentals. Leipziger Universitätsverlag, Leipzig (2005). ISBN ISBN: 3-86583-073-0
30. Laidlaw, I., Steinmetz, M.: Introduction to differential sedimentation. In: Scott, D.J., Harding, S.E., Rowe, A.J. (eds.) Analytical Ultracentrifugation Techniques and Methods, pp. 270–290. Royal Society of Chemistry, Cambridge (2005)
31. Lange, H.: Comparative test of methods to determine particle size and particle size distribution in the submicron range. Part. Part. Syst. Charact. **12**(3), 148–157 (1995)
32. Lett, J.T.: Measurement of single strand breaks by sedimentation in alkaline sucrose gradients. In: Friedberg, E.C., Hanawalt, P.C. (eds.) DNA repair – A Laboratory Manual of Research Procedures, vol. 1, pp. 363–378. Marcel Dekker, New York (1981)
33. Mende, S., Stenger, F., Peukert, W., Schwedes, J.: Mechanical production and stabilization of submicron particles in stirred media mills. Powder Technol. **132**, 64–73 (2003)
34. Mura, P., Faucci, M.T., Parrini, P.L.: Effects of grinding with micro-crystalline cellulose and cyclodextrins on the ketoprofen physicochemical properties. Drug Dev. Ind. Pharm. **27**, 119–128 (2001)
35. Noyes, A.A., Whitney, W.R.: The rate of solution of solid substances in their own solutions. J. Am. Chem. Soc. **19**, 930–936 (1897)
36. Ouattara, B., Simard, R.E., Piette, G., Begin, A., Holley, R.A.: Diffusion of acetic and propionic acids from chitosan-based antimicrobial packaging films. J. Food Sci. **65**, 768–773 (2000)
37. Ozdemir, J.D.: Floros, analysis and modeling of potassium sorbate diffusion through edible whey protein films. J. Food Sci. **65**, 149–155 (2001)
38. Ozdemir, M., Floros, J.D.: Film composition effect on diffusion of potassium sorbate through whey protein films. J. Food Eng. **68**, 511–516 (2003)
39. Perez-Gago, M.B., Krochta, J.M.: Water vapor permeability of whey protein emulsion films as affected by pH. J. Food Sci. **64**, 695–698 (1999)
40. Redl, A., Gontard, N., Guilbert, S.: Determination of sorbic acid diffusivity in edible wheat gluten and lipid based films. J. Food Sci. **61**, 116–120 (1996)
41. Redner, S.: Statistical model for the fracture disordered media. In: Hulin, J.P. (ed.) Fragmentation, pp. 321–328. Elsevier, London (1990)
42. Saito, M., Ugajin, T., Nozawa, Y., Sadzuka, Y., Miyagishima, A., Sonobe, T.: Preparation and dissolution characteristics of griseofulvin solid dispersions with saccharides. Int. J. Pharm. **249**, 71–79 (2002)
43. Teerakarn, A., Hirt, D.E., Action, J.C., Rieck, J.R., Dawson, P.L.: Nisin diffusion in protein films: Effect of film type and temperature. J. Food Sci. **67**(8), 3019–3025 (2002)
44. Varinot, C., Hiltgun, S., Pons, M.-N., Dodds, J.: Identification of the fragmentation mechanisms in wet-phase fine grinding in a stirred bead mill. Chem. Eng. Sci. **52**(20), 3605–3612 (1997)
45. Vippagunta, S.R., Maul, K.A., Tallavajhala, S., Grant, D.J.: Solid-state characterization of nifedipine solid dispersions. Int. J. Pharm. **236**, 111–123 (2002)

46. Vojdani, F., Torres, J.A.: Potassium sorbate permeability of methyl-cellulose and hydroxypropyl methyl-cellulose coatings: Effect of fatty acids. J. Food Sci. **55**, 841–846 (1990)
47. Warin, F., Gekas, V., Voirin, A., Dejmek, P.: Sugar diffusivity in agar gel/milk bilayer systems. J. Food Sci. **62**, 454–456 (1997)
48. Yamada, T., Saito, N., Imai, T., Otagiri, M.: Effect of grinding with hydroxypropyl cellulose on the dissolution and particle size of a poorly water-soluble drug. Chem. Pharm. Bulletin **47**, 1311–1313 (1999)